PERGAMON

Journal of Structural Geology 22 (2000) 1427–1435

JOURNAL OF STRUCTURAL GEOLOGY

www.elsevier.nl/locate/jstrugeo

New fractographic aspects of natural and artificial fractures in chalks from the Upper Galilee, Israel, and experimental fracture in Perspex

Dov Bahat[a,*], Avinoam Rabinovitch[b]

[a]*Department of Geological and Environmental Sciences, Ben-Gurion University of the Negev, Beer Sheva 84105, Israel*
[b]*Physics Department, Ben-Gurion University of the Negev, Beer Sheva 84105, Israel*

Received 12 May 1999; accepted 5 May 2000

Abstract

The fractographies of an artificial fracture that was formed by a blast and a natural fracture cutting chalks that display mirror planes and hackled fringes are similar. In both fractures the mirror and fringe are separated by clear boundaries, and the locations of the maximum hackle intensity and maximum ϕ angle (produced between the mirror plane and the fringe) coincide with the positions where segments of the mirror boundaries that have different curvatures meet. On both the natural and artificial fractures, radial hackles associated with the different boundary segments focus on distinct origins. The ϕ angle varies from 0° to $30^\circ \pm 5^\circ$ on the natural joint and from $30^\circ \pm 8^\circ$ to $50^\circ \pm 8^\circ$ on the artificial fracture. The coinciding positions of hackle intensity and ϕ maxima observed in the two fractures match well with bifurcating fractures induced by experimental Hertzian fracture in Perspex. These are further supported by a geometric mismatch analysis. The present results demonstrate that the K_I increases, which occur in positions where fractures of different ellipticities meet, enhance hackle intensity, crack-branching and the value of ϕ.

1. Introduction

1.1. General

Fractures that develop both artificially and in nature often display asymmetric mirror planes that represent mergers of earlier smaller cracks (Bahat et al., 1999). The early cracks may propagate independently under different local stresses and will have different velocities. Therefore, their boundaries commonly differ in curvature, and when they coalesce their mirror boundaries may not lie on the same arc. Such geometrical differences may also occur when the propagation of a single crack is disturbed by heterogeneous boundary conditions. Our results show that stress was concentrated at the junctions between mirror boundaries with different geometries. The present study relates to the effects of this stress concentration increase on fracture via the combined observations made on artificial and natural fractures, supplemented by fracture experimentation on Perspex and by a mathematical analysis.

1.2. Classification

Joints that have fringes (Hodgson, 1961) may be divided into distinct groups according to the following criteria:

1. Sharp boundaries between the parent joint and the fringe vs. non-sharp boundaries between the two (i.e. discontinuous vs. continuous transition from the planar joint to the en échelon fringe, respectively, Bahat, 1986).
2. Fringes consisting of en échelon segments vs. fringes populated by hackles (Bahat, 1986).
3. Natural vs. artificial joints (Bahat, 1991, p. 209).

* Corresponding author. Fax +972-7-6472-997.
E-mail address: bahat@bgumail.bgu.ac.il (D. Bahat).

0191-8141/00/$ - see front matter
PII: S0191-8141(00)00055-9

Representatives of these groups are presented below.

1.3. Discoids with sharp and non-sharp boundaries

Woodworth (1896) observed the tendency of joints in some argillaceous rocks to develop into warping or curving discoid shapes. Bankwitz (1966) described discoid-like smooth, rounded joints in slates (Fig. 1a). These structures often occur in clusters where fringes of radial en échelon and step fractures are rotated with respect to the circular parent joint (Fig. 1b). Occasionally rotated fringes are also twisted (Fig. 1a), which suggests that they deformed plastically (Bahat, 1991, p. 189). However, there are also discoids that show sharp and angular boundaries between the flat parent joint and untwisted fringes (Fig. 1b and c) suggesting that their deformation occurred in considerable rigidity by brittle fracture. A characteristic feature of discoids and some non-sedimentary rocks (like granite) is that their fringes are large compared to the size of the parent joint.

1.4. En échelon vs. hackle fringes on natural joint surfaces

En échelon fringes of non-discoid joints that occur in sedimentary rocks and develop by brittle deformation are typically considerably smaller than the parent joints, and fringes are coplanar with the surface of the parent joint (Fig. 1d). It is considered that most

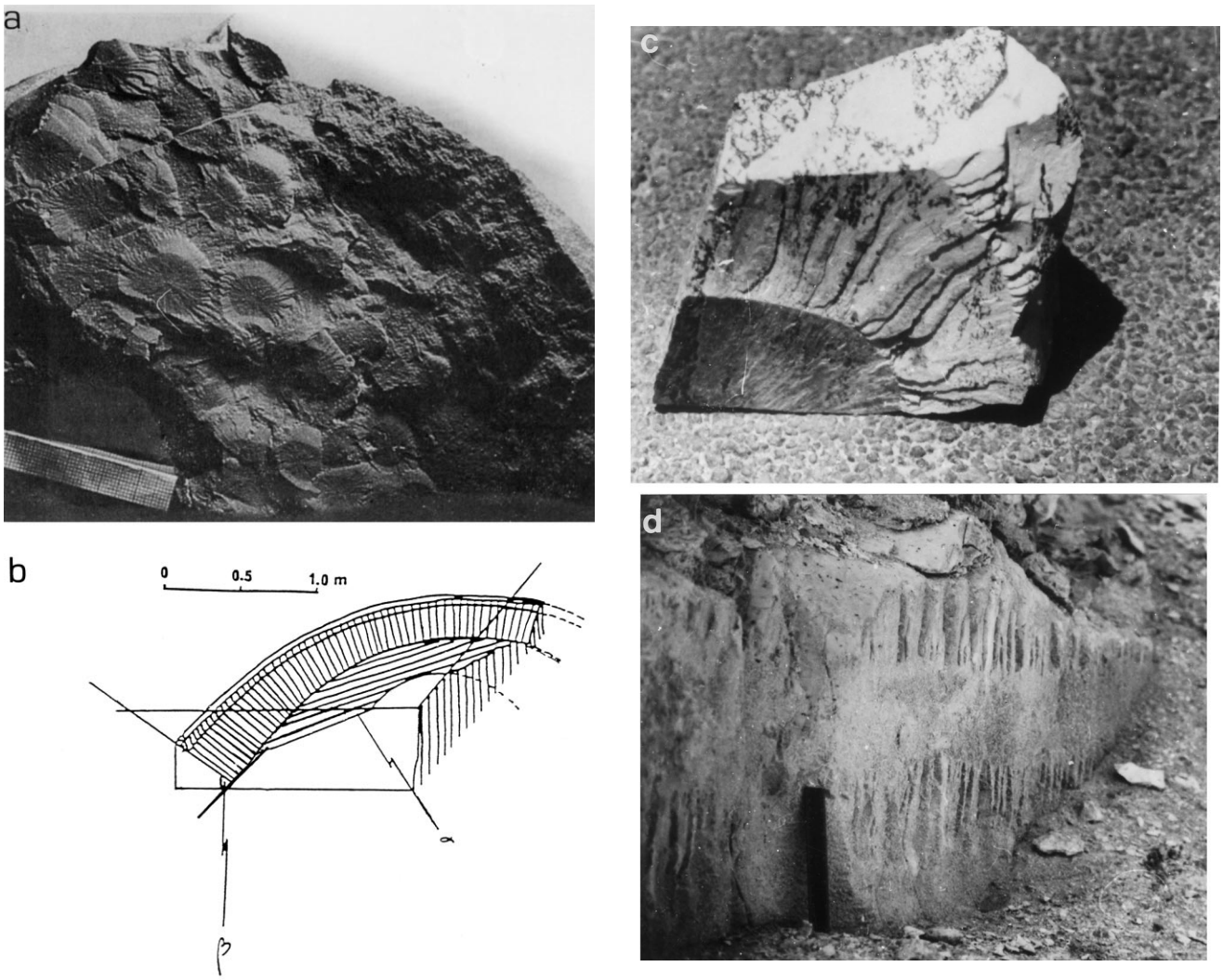

Fig. 1. (a) 'Eye' discoid joints in Ordovician Frauenbach Quarzite of the Thuringian Schiefergebirge (from Bankwitz and Bankwitz, 1984). (b) A schematic discoid, showing the angles of deviation α between the parent fracture and various fracture planes of the fringe, and the kink angles β between these fringe planes (modified after Bankwitz, 1966).(c) Fragment of a conic discoid from the Ramon flint clay. A curved shoulder separates between the flat parent joint (lower left) and the fringe of first-stage en échelon cracks (upper right). The second stage en échelon fringe is just visible at the upper right corner of discoid. Scale is 12 cm. (d) Vertical joint cutting chalk in the Beer Sheva syncline, southern Israel, with a parent region at the centre, and en échelon fringes above and below it. Scale is 15 cm.

joints were formed by sub-critical processes, i.e. at low fracture velocities (e.g. Kendall and Briggs, 1933). This concept is based on the observation that joints cutting sedimentary rocks generally do not have hackled fringes (Fig. 2a) and do not bifurcate (unless they are associated with intense tectonic processes, Bahat et al., 1999). The latter are accepted criteria for intense fracture, i.e. fracture which occurs either rapidly or under high values of the tensile stress intensity factor K_I (some authors erroneously equate the two, not realizing that fracture velocity is not necessarily a single valued function of K_I). Fringes of many joints however, consist of en échelon segments (Fig. 2b).

1.5. Artificial fractures

When glassy materials fracture they typically form mirror planes rimmed with hackled fringes (Fig. 2a). However, when grain boundaries distort the 'glassy-optimal' hackles in ceramics and blasted rocks, ridges and grooves called 'cuspate hackles' are formed (Bahat, 1991, p. 181). These markings are caused by conventional explosive techniques as practised in quarries, road cutting and other construction works. Cuspate hackles characteristically display series of alternating sharp ridges and grooves, both of nearly constant width, that are approximately radial with respect to the origin, which is located on the mirror plane (Figs. 2a and 3a). Some artificial fractures display an angular relationship between the parent joint and the fringe along their boundary.

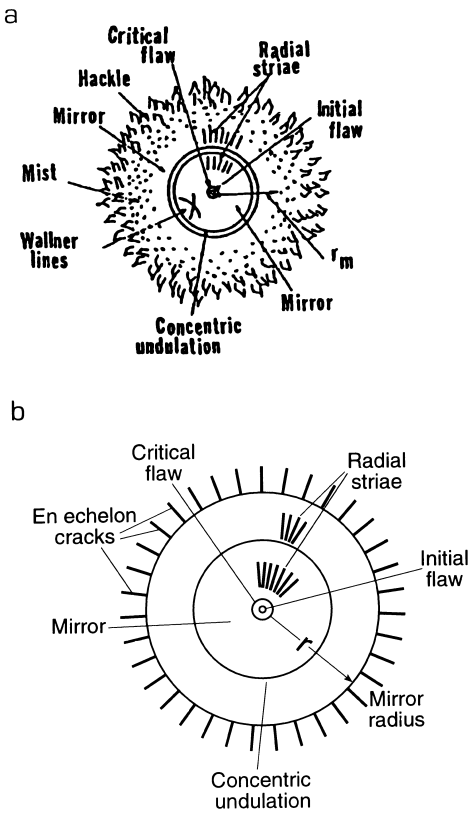

Fig. 2. (a) Schematic representation of a fracture surface caused by an intense fracture in glass (e.g. Bahat et al., 1982), showing the fracture origin (pre-existing flaw), the critical flaw, mirror plane, radial striae, concentric undulations (ripple marks), Wallner lines, mist, hackle, and r_m the mirror radius. (b) Schematic representation of a fracture surface showing similar features to those in (a), with three differences: Wallner lines and mist are omitted and hackles are replaced by en échelon cracks.

1.6. Natural joints that resemble artificial fractures

There are rare (natural) joints in sedimentary rocks that display fractographic features similar to those displayed by rapidly fractured ceramics in the laboratory and blasted rocks in the field. The present study focuses on the fracture morphologies of artificial and natural fractures which exhibit resembling features of mirror planes and hackled fringes. These fractures display measurable angular relations between the planes and fringes along their mutual boundaries.

2. Fractography

2.1. General

Quantitative fractography is based on the empirical relationship $\sigma_f r^{1/2} = A$, where σ_f is the fracture stress, r is the mirror radius and A is the mirror fracture mechanical constant. Accordingly, r is reduced with the intensity of the fracture. Therefore, mirror plane radii formed by quarrying techniques are small relative to hackle lengths in the fringes because of fracturing under high stresses. However, in natural fractures formed by relatively low stresses, when hackles occur, they are relatively short and radiate from a mirror perimeter of a relatively large radius. This difference is clearly displayed in the two examples under the present investigation (Fig. 3a–d). The fractures in Fig. 3(a and b) were formed under high-stress and low-stress conditions, respectively.

2.2. The Ma'alote artificial fracture

The Ma'alote artificial fracture that was formed by a blast (Bahat, 1991, p. 208) cuts Cenomanian chalk near Ma'alote in the Upper Galilee. The arc of the quasi-elliptical mirror boundary is convex upward indicating an upward fracture propagation. The curvature of this boundary, however, is not uniform and may be divided at m into two segments that differ in their curvature and which do not lie on the same arc (Fig. 3a and c). Most of the boundary is fairly uniformly curved (to the left of m). However, about a fifth of the

boundary, on the right-hand side of m is rather straight. The hackles on the right side of m show greater 'hackle intensity', than those on the left-hand side of m: The right-hand ones are longer, wider and cut deeper into the rock. The hackles on the left-hand side of m focus at f, whereas the hackles on its right-hand side deviate from this radial orientation, focusing on g (Fig. 3c). None of these foci coincides with the fracture origin at o, but f is closer to it then g. The ratio of hackle length (the distance qm)/mirror radius (the om distance) is ~ 1.

The ϕ angle produced between the mirror and fringe varies from $30^\circ \pm 8^\circ$ to $50^\circ \pm 8^\circ$ along the mirror boundary. It reaches its maximum along the straight segment of the boundary, close to point m where the two segments meet. This maximum coincides with the location of maximum hackle intensity (Fig. 3c).

2.2.1. The Safad natural joint

The Safad natural joint cuts Senonian chalk near Safad in the Upper Galilee. This joint has been removed from the outcrop and brought to the laboratory, and its original propagation direction was not recorded.

There is a clear distinction along the mirror boundary between the mirror (light) and the fringe (dark) (Fig. 3d, note that Fig. 3b and d were taken under different light conditions). The mirror plane is divided along the imaginary line between m and o into two unequal parts (Fig. 3d). The larger part on the right side is marked by a faint radial set of striae (plumes) with a superposing series of concentric undulations that display an orthogonal relationship with the plumes at each intersection between the two. Both striae and undulations focus on a single origin, o (see r_1 in Fig. 3d). The plumes in the smaller part at left and their matching undulations continue their orientations from the larger part (Fig. 3b), together focusing on the common origin o (see r_2).

The mirror boundary is divided into two segments

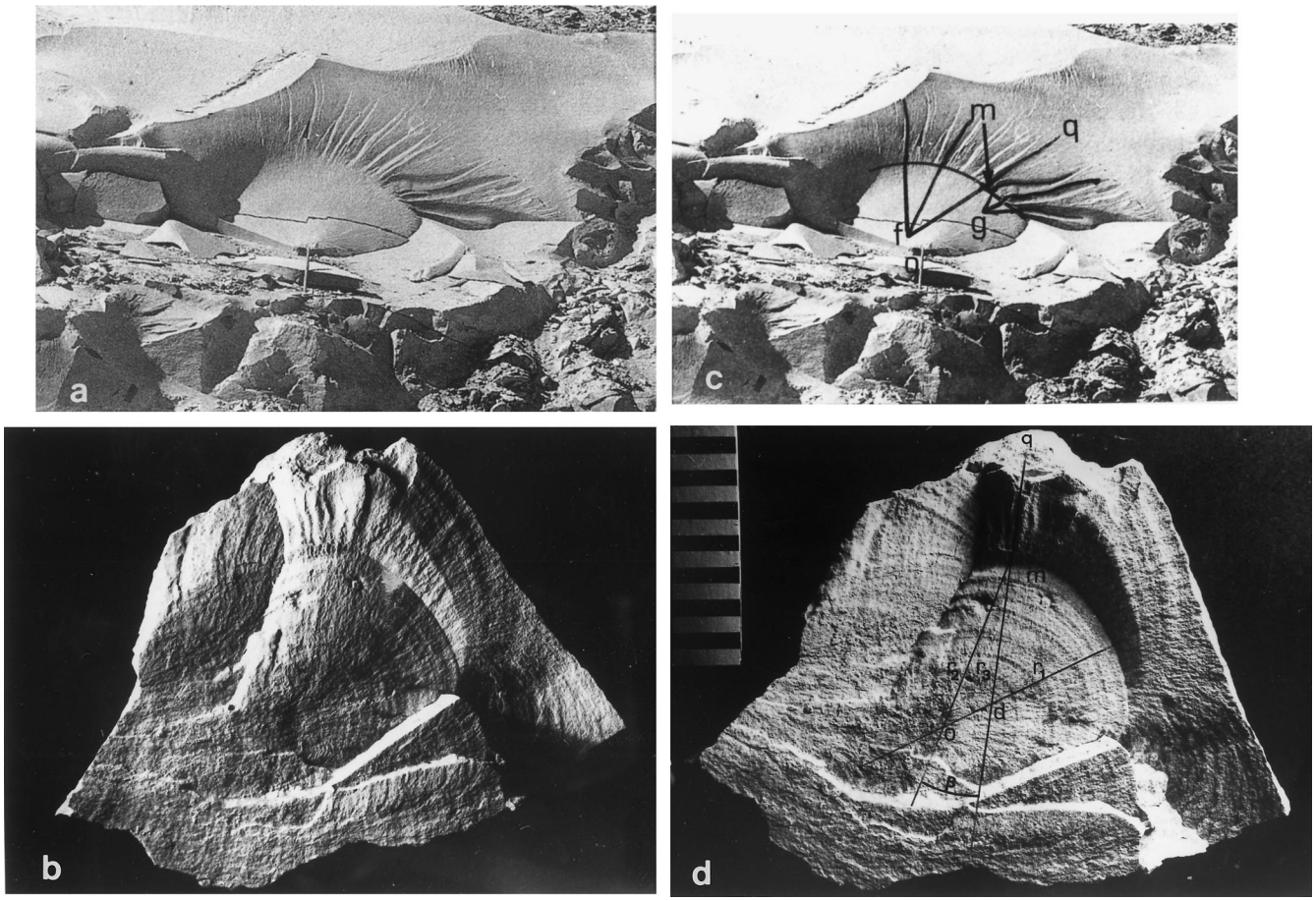

Fig. 3. (a) A mirror and long radial hackles in a ruptured chalk along a road quarry (Cenomanian, Upper Galill, near Ma'alote). Typical length of hackles in this outcrop approximates the radial length of the mirror plane. (b) Fracture surface of a joint cutting Senonian chalk near Safad from the Upper Gaglill in northern Israel, showing the curved and sharp boundary separating the mirror plane from the fringe. (c) Drawing superposed on (a), showing m, the location where the two segments of mirror boundary merge and the two foci, f and g, where the hackles of both parts of the fringe meet. A 15 cm bar marks the point of fracture origin at o. (d) Superposition of a drawing on a photograph of the Safad joint that was taken from a different angle compared to that shown in (b). See explanation in text.

that differ from each other in length, curvature and orientation. The shorter segment at left is straighter and the longer one at right is curved, both meet at m (Fig. 3b and d).

The hackles in the fringe, along the longer boundary segment continue the radial orientation of the striae from the larger mirror part (r_1 in Fig. 3d). On the other hand, the hackles along the shorter segment differ in their orientation from the other hackles and from all striae, and they focus on a different location at d (see r_3), which is to the right of o. The angle produced at the mirror boundary at m by the radii initiating at d and o is $\beta = 11^\circ \pm 1.5^\circ$. Note that whereas in the Ma'alote fracture the foci of the two hackle groups (f and g) deviate from the origin, o, in the Safad joint only the focus of the more intense hackles deviates from o.

There are gradual increases in the hackle intensities from the two ends of the mirror boundary towards point m, where the two segments of the boundary meet (Fig. 3b and d). Generally, the hackles next to the straighter segment at left, are more intense than those next to the longer segment, reaching maximum close to m. The ratio of hackle length (qm)/mirror radius (om) along the line omq is $\sim 1/2$. This ratio is about half the corresponding one on the Ma'alote artificial fracture (Fig. 3d and b, respectively). There is a narrow belt of 'micro-hackles' exclusively along the straighter boundary segment (Fig. 3b) that resembles the 'root zone' (Bankwitz, 1966) of micro en échelon segments.

The ϕ angle produced between the mirror and fringe (Fig. 3d) varies along the mirror boundary from 0° at the right end of the fringe to $30^\circ \pm 5^\circ$ close to point m where the two segments meet, coinciding with the location of maximum hackle intensity.

Hence, in both fractures (Fig. 3a–d) the locations of highest hackle intensity and of ϕ maxima do not fall at the arch centres, where the arches are best developed (corresponding to ellipticity minima). They rather occur along the straighter parts of the mirror boundaries (where $r \to \infty$), and particularly close to m (Fig. 3b and d).

3. Experimental method

Two distinct fracture morphologies of Herzian fracture (Frank and Lawn, 1967) that were obtained by hydraulic means, are presented below. In each of the two experiments grease was the hydraulic medium. Pressure was rapidly applied by a steel piston through an axial borehole drilled into Perspex cylinders 42 mm high and 48 mm in diameter (Bahat, 1991, p. 136). The fracture surfaces that developed in the two experiments were divided into five zones: (1) The initial crack at the bottom of the borehole; (2) an initial subvertical ring, about 0.2 mm thick (hardly visible in the sample); (3) a conic fracture that was marked by concentric delicate undulations; in this zone the conic angle θ (produced between the conic axis and the conic fracture) was uniform around the initial circular crack; (4) a flat surface that continued the cone and was marked by delicate radial 'striae' that propagated from the centre towards the sample periphery; and (5) an outer concentric rim between zone 4 and the edge of the sample (Fig. 4a). In some experiments zone 4 reached the sample periphery and zone 5 was missing.

In the second experiment both borehole and piston were elliptical, such that the aspect ratio of large diameter/small diameter was 1.5 (Fig. 4b). The fracture surface that developed was divided into the same four or five zones as in the first experiment. However, two differences were noticeable. First, the initial elliptical crack (zone 1) developed into an elliptic conic fracture (zone 3), and the conic angle θ was not uniform around the initial elliptical crack: It was deeper on both sides of zone 1, 'sub-parallel' to the elliptical major axis $2a$ ($50^\circ \pm 5^\circ$) and more moderate on both sides of zone 1, 'sub-parallel' to the elliptical minor axis $2b$ ($35^\circ \pm 5^\circ$). Consequently, an undulatory topography developed on the fracture surface of zone 4, such that the highest elevations along the conic and flat zones on both sides of the diameter a were several millimetres higher than the lowest elevations on both sides of the diameter b (Figs. 4c and 5). Second, additional fractures developed as well. Radial 'branching cracks' advanced from four locations at the boundary between zones 4 and 5 towards the centre of the sample and arrested at the boundary between zones 3 and 4, i.e. they were confined to the undulatory surface. The reverse propagation direction was identified by the branching style, whereby the branches faced zone 1, which is the characteristic feature of crack branching (Fig. 4d) (see further discussion in Section 5). The branching cracks concentrated along four 'radial strips', each one about 4–10 mm wide (differing from sample to sample), that coincided with the inflection positions on the undulatory topography (Fig. 4c). In this configuration, the semi-axis a of the initial ellipse bisected two small angles (each with $2\varphi \approx 85^\circ$), and semi-axis b of the initial ellipse bisected two large angles (each with $180^\circ - 2\varphi \approx 95^\circ$) (Fig. 4d).

4. Analysis of the location of maximum curvature mismatch on the ellipse

The fractures in zones 3 and 4 (Fig. 4b and d) developed into elliptic shapes due to the influence of the ellipticities of the initial cracks forming the ellipse of zone 1.

Consider an ellipse of major dimension $2a$ and minor dimension $2b$ (Fig. 5). A point (x, y) on the ellipse is given either by the equation

$$x^2/a^2 + y^2/b^2 = 1,$$

or by the parametric equations

$$x = a \cos t$$

$$y = b \sin t,$$

where t is a parameter measuring position along the ellipse. The radius of curvature R, of any function $y(x)$ at the point (x, y) is given by

$$R = \left|1 + y'^2\right|^{\frac{3}{2}} / \left|y''\right|$$

and for an ellipse:

$$R = (a^2 \sin^2 t + b^2 \cos^2 t)^{3/2}/ab,$$

the rate of change of R with respect to t is given by

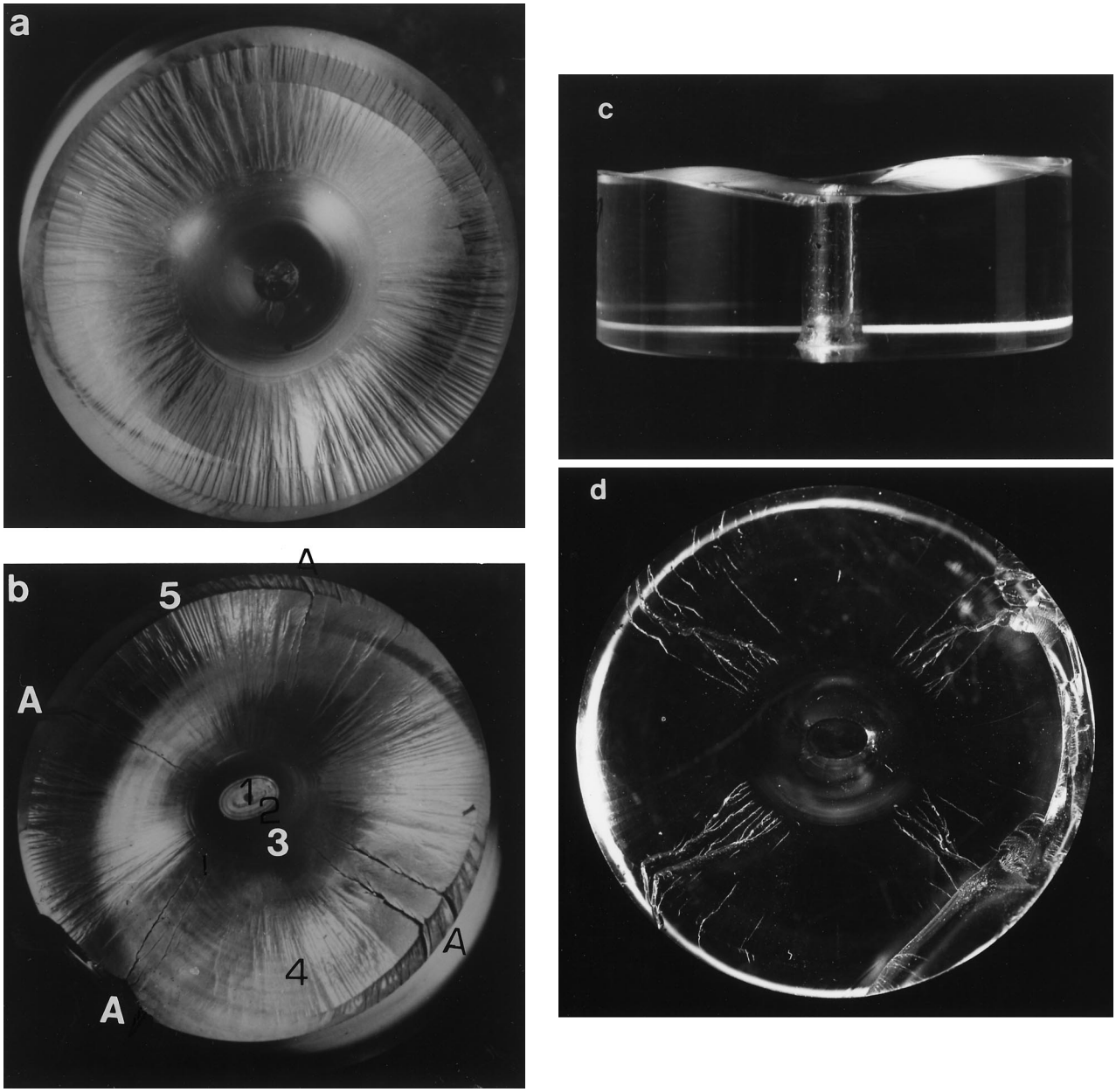

Fig. 4. Fracture markings in Perspex cylinders 42 mm high and 48 mm in diameter fractured by hydraulic pressure. In (a) borehole and piston were circular, in (b) borehole and piston were elliptical, numbers 1–5 differentiate five zones, points A signify locations of 'radial strips'; they correspond to A locations in Fig. 5, (c) a profile of the Herzian fracture (zones 3–5) showing the undulatory topography. (d) Branching in four radial strips faces zone 1 (experiments shown in b and d are different).

$dR/dt = 3/2(a^2 \sin^2 t + b^2 \cos^2 t)^{1/2} (a^2-b^2)/ab \sin 2t.$

This is a measure of the mismatch of curvature. It measures in effect the change in the radius of curvature between two adjacent points on the ellipse. We are interested in the point at which the mismatch is maximum. For that we equate to zero the second derivative, $d^2R/dt^2 = 0$, to obtain t_m, the value of t for which dR/dt is maximal (note that the exact value should have been $d^2R/d\varphi^2 = 0$, where $\varphi = \arctan y/x$. However, since $dt/d\varphi$ is never zero, this is equivalent to $d^2R/dt^2 = 0$). This yields,

$\sin^2 t_m = [2-\alpha \pm (1-\alpha+\alpha^2)^{1/2}]/3(1-\alpha)$

where $\alpha = a^2/b^2$. The value t_m defines the maximum mismatch angle φ_m on the ellipse according to

$\tan \varphi_m = (b/a) \tan t_m = \alpha^{-1/2} \tan t_m.$

Fig. 5 depicts a specific example of an ellipse with the four largest mismatch angles $A(\varphi_m)$.

Previous calculations of paleostress magnitudes showed the need to treat especially mirror boundaries with elliptical deviations from circularity (Bahat et al., 1999). In fact, the ellipticities of many geological circular structures vary considerably. For instance, the classic idealized geological map of an alkalic–ultramafic–carbonatitic cone-sheet drawn by Heinrich (1966) (Figs. 2–5) is an ellipse (Fig. 6). Quite intriguing is the fact that this map contains radial dikes at the four locations that approximate the positions of the radial 'branching cracks' (Fig. 4d). The radial dikes also resemble the radii at A that produce the φ_m angle in Fig. 5.

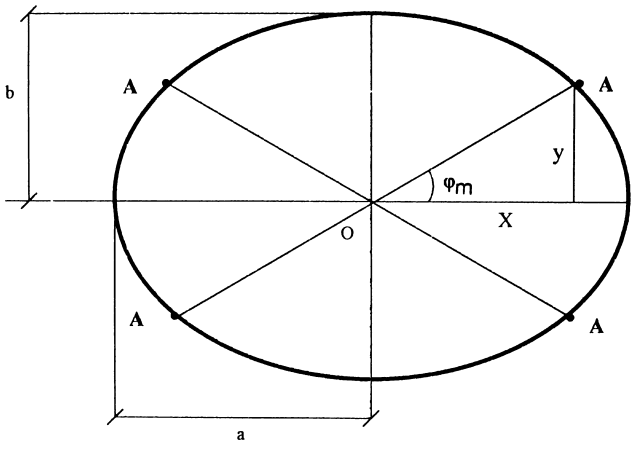

Fig. 5. Ellipse of major dimension $2a$ and minor dimension $2b$. Points A mark the locations, and φ_m is the angle, for which the mismatch (dR/dt) is a maximum.

5. Discussion

5.1. General

The 'stress-intensity criterion' states that the mirror boundaries with the mist, hackle or branching initiation (Fig. 2a and b) will form when the local appropriate stress intensity factors K_I, reach their critical values K_{Im}, K_{Ih}, K_{Ib}, respectively (Clark and Irwin, 1966; Congleton and Petch, 1967; Bahat et al., 1982; Kirchner and Conway, 1987). The literature on engineering materials generally concerns the three boundaries and their corresponding K_I values (e.g. Kirchner and Conway, 1987). Due to lack of mist on geological fracture surfaces, geological interest generally concentrates on K_{Ih} and K_{Ib}. However, the interpretation of our current observations requires that we add a new K_I, as will be explained in the next paragraph.

5.2. Concentric tension on the joint surfaces

The two segments of the mirror boundary on the Safad fracture differ in their lengths and in their curvatures, and the hackles originating from these segments are differently oriented (Fig. 3a and c). The same differences apply to the Ma'alote fracture (Fig. 3b and d). Quite possibly the propagation of the Safad and Ma'alote fractures was affected by the shape of the countryrock around them, in analogy to the influence of layer-boundaries on the propagation of plumes along the layers (Bahat, 1991).

In both the Safad and Ma'alote fractures the two parts of the mirror fanned out radially so that they

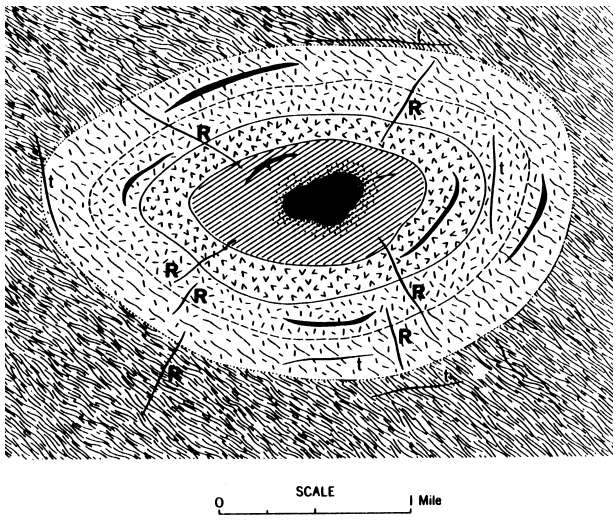

Fig. 6. Idealized geological map of an elliptic carbonatitic cone-sheet, showing various concentric alkalic–ultramafic rock series fractured by tangential, t and radial, R dikes. The latter strongly resemble the A radii in Fig. 4(b) and the A radii in Fig. 5 (modified from Heinrich, 1966).

produced distinct fans of hackles in the fringes. This fanning also caused an 'opening' between the two parts, which increased with the radius. Note that this 'opening' was concentric on the joint surfaces, being normal to the opening producing the joints by the original tensile stress. The new 'opening' was associated with a local concentric tensile stress and a new K_I, denoted hereafter by $K_I^{(n)}$ orthogonal to the original K_I.

5.3. The reflection of $K_I^{(n)}$ by maxima in hackle intensity and in ϕ

In both the Safad and Ma'alote fractures the locations of maximum ϕ and maximum hackle intensity coincide close to point m (Fig. 3c and d, respectively), implying a strong correlation between these two features. Since K_I, to a large extent (not exclusively, Lawn and Wilshaw, 1975) controls secondary fracture in the fringe, it is a major contributor to the high hackle intensity. Following the discussion in the previous paragraph, hackles start to develop when $K_I = K_{Ih}$, and, we maintain that the maximum hackle intensity is obtained at the locations where the $K_I^{(n)}$ occurs. K_I and $K_I^{(n)}$ are superposed around these locations.

5.4. The location of maximum curvature mismatch on the ellipse

The bifurcation of the branches along the four radial fractures (Fig. 4b and d) resulted by the local maximum tensile stress, σ_1, orthogonal to each branching crack in its respective radial strip. The original σ_1 was normal to the fracture plane in zones 3 and 4 (sub-parallel to the sample axis) during the Herzian primary fracture (Lawn and Wilshaw, 1975). However, the new σ_1 was rotated by 90° and has assumed a concentric orientation when the radial fractures initiated their reversed propagation from the boundary between zones 4 and 5 towards the centre of the sample.

Döll and Weidmann (1976) measured the crack velocity as a function of stress intensity factor, and determined the transitions from slow to fast crack propagation in PMMA of two different molecular weights (8,000,000 and 115,000). The transitions at room temperature were abrupt from about 0.1 m/s at the end of the slow propagation region to about 10 to 100 m/s at K_{Ic} values (56.1 ± 3.6 and 38.5 ± 2.0 Nm $m^{-3/2}$, respectively). These transitions were accompanied by corresponding abrupt changes in the fracture surface morphologies. The slow crack propagation region was rough, consisting of series of delicate 'river-lines' that lay sub-parallel to the direction of propagation. Beyond sharp boundaries smooth surfaces represented the high-velocity region.

In our samples (Fig. 4) the smooth surface (zone 3) preceded the rough one (zone 4). Therefore, the results of Döll and Weidmann, (1976) imply that in our experiment the fracture of the smooth cone occurred at the maximum velocity, which was later reduced while forming the rough fracture. It is unlikely that the bifurcating fractures that coincide in their location with the rough surfaces were developed under stress intensity conditions that were associated with low fracture velocity. This adds support to our assertion that the bifurcating fractures did not start at the boundary between zones 3 and 4 (Fig. 4b), but rather, propagated from the periphery of the sample towards the centre.

Furthermore, points A (Fig. 5) are located approximately at the positions of maximum curvature mismatch and repeated branching along the strips of radial fractures in Fig. 4(b and d). We however, interpret the deviations from exact fitting of the radial strips (Fig. 4b) to the A locations, to stresses exerted by the undulatory topography (Fig. 4c) and to actual slight deviation of the initial elliptical crack (zone 1) from an exact ellipse (Fig. 4b). Branching evidently designates the condition where $K_I^{(n)} \geq K_{Ib}$.

We suggest the following fracture scenario: after the elliptical conic fracture had formed by the compressive shock pulse generated by the indentation, the reflected tensile stress waves propagated backwards from the cylindrical boundary (Field, 1971) towards the initial elliptic crack. These waves include a 90° rotation component due to the geometric mismatch and induced back fractures along four strips for $K_I^{(n)} > K_{Ic}$, which later branched when $K_I^{(n)} \geq K_{Ib}$. Cracks in these strips propagated approximately towards the loci of 'maximum elliptical mismatch' at the initial elliptic crack (A in Figs. 4b and 5).

5.5. Future research

The correlations introduced in this study between: (a) the location of maximum curvature mismatch, (b) the location of maximum hackle intensity, (c) joint multi-stage growth and the β angle, (d) the conditions that affect differences between various ψ angles, and, (e) the conditions that affect variations in the ϕ angle along the mirror boundary, need to be further explored and also correlated with the role of the θ angle in influencing these parameters. This will further enlarge the knowledge and understanding of fracture processes on mirror planes and on fringes of joints.

A further mathematical development of the concept of 'maximum elliptical mismatch' may have additional applications in structural geology. For instance, failure processes of large (e.g. De Sitter, 1962) and small asymmetric folds at their crests would be quantitatively analysed.

6. Summary

A distinction is made between different groups of joints that have fringes, according to three criteria: The extent of sharpness of boundaries between the parent joint and the fringe, en échelon segments vs. hackles in the fringe, and, natural vs. artificial joints.

The fractographies of an artificial and a natural fracture cutting chalks that display mirror planes and hackled fringes are surprisingly similar. In both fractures the maximum hackle intensity and maximum ϕ (the angle produced between the mirror plane and the fringe) coincide with the positions where distinct segments of the mirror boundaries with different curvatures meet.

Experimental results of Herzian fracture induced by an elliptical indenter show zones of $K_{\mathrm{I}}^{(\mathrm{n})}$ (the K_{I} which is orthogonal to the original K_{I}) increases and crack bifurcations that approximately coincide with locations on the ellipse that have the highest rate of change of the radius of curvature. The matching of results from natural and artificial fractures, supported by observations from induced fracture in the laboratory, suggest that $K_{\mathrm{I}}^{(\mathrm{n})}$ increases occur in positions where fractures of different ellipticities meet. The increase in $K_{\mathrm{I}}^{(\mathrm{n})}$ enhances hackle intensity, back cracking, crack-branching and the value of ϕ.

Acknowledgements

We would like to thank Peter Bankwitz, an anonymous reviewer and Tom G. Blenkinsop for most useful comments on an earlier version that helped to considerably improve the paper.

References

Bahat, D., 1986. Criteria for the differentiation of en echelons and hackles in fractured rocks. Tectonophysics 121, 197–206.

Bahat, D., 1991. Tectonofractography. Springer-Verlag, Heidelberg.

Bahat, D., Leonard, G., Rabinovitch, A., 1982. Analysis of symmetric fracture mirrors in glass bottles. International Journal of Fracture 18, 29–38.

Bahat, D., Grossenbacher, K., Karasaki, K., 1999. Mechanism of exfoliation joint formation in granitic rocks, Yosemite National Park. Journal of Structural Geology 21, 85–96.

Bankwitz, P., 1966. Ueber Kluefte. II. Die Bildung der Kluftflaeche und eine Systematik ihrer Strukturen. Geologie 15, 896–941.

Bankwitz, P., Bankwitz, E., 1984. Die Symmetrie von Kluftoberflaechen und ihre Nutzung fuer eine Palaeospannungsanalyse. Zeitschrift fuer Geologische Wissenshcaften 12, 305–334.

Clark, A.B.J., Irwin, G.R., 1966. Crack propagation behaviors. Experimental Mechanics 6, 321–329.

Congleton, J, Petch, N.J., 1967. Crack branching. Philosophical Magazine 16, 749–760.

De Sitter, L.U., 1962. Structural development of the Arabian shield in Palestine. Geologie en Mijnbouw 41, 116–124.

Döll, W., Weidmann, G.W., 1976. Transition from slow to fast crack propagation in PMMA. Journal of Materials Science (Letters) 11, 2348–2350.

Field, J.E., 1971. Brittle fracture: its study and application. Contemporary Physics 12, 1–31.

Frank, F.C., Lawn, B.R., 1967. On the theory of Hertzian fracture. Proceedings of the Royal Society A 299, 291–306.

Hodgson, R.A., 1961. Regional study of jointing in comb ridge—Navajo Mountain area, Arizona and Utah. American Association of Petroleum Geologists Bulletin 45, 1–38.

Heinrich, E. Wm., 1966. The Geology of Carbonatites. Rand McNally & Company, Chicago.

Kendall, P.F., Briggs, H., 1933. The formation of rock joints and the cleat of coal. Proceedings of the Royal Society 53, 164–187.

Kirchner, H.P., Conway Jr, J.C., 1987. Comparison of the stress-intensity and Johnson-and-Holloway criteria for crack branching in rectangular bars. Journal of the American Ceramic Society 70, 565–569.

Lawn, B.R., Wilshaw, T.R., 1975. Fracture of Brittle Solids. Cambridge University Press, London.

Woodworth, J.B., 1896. On the fracture system of joints, with remarks on certain great fractures. Boston Society of Natural History Proceedings 27, 63–184.